On the impact of beamforming strategy on mm-wave localization performance limits

On the Impact of Beamforming Strategy on mm-Wave Localization Performance Limits

Anna Guerra, *Member, IEEE,* Francesco Guidi, *Member, IEEE,* Davide Dardari *Senior Member, IEEE*

***Abstract*—In this paper we investigate the localization performance limits of massive arrays working at millimeter-wave (mm-wave) frequencies and adopting two different beamforming strategies. In the first one, array weights are set in order to point towards a precise direction (*classic beamforming*), whereas in the second one, such weights are randomly chosen (*random beamforming*). Thanks to the large set of measurements as well as the high angular resolution provided by massive arrays, only one single anchor node can be used for localization estimation, thus avoiding over-sized infrastructures dedicated to positioning. Accounting for such beamforming strategies, performance is evaluated by taking into account the effects of arrays orientation and beamforming weights non-idealities arising when the number of antennas is high and low-complex components are adopted. Results reveal that classical beamforming outperforms the random one which still remains a feasible solution when the system complexity has to be kept affordable.**

***Index Terms*—Position Error Bound, Millimeter-wave, Massive array, 3D localization.**

I. Introduction

Fifth generation personal devices will be required to perform self-localization in indoor environments as well as to share a huge amount of data at extremely high rates [1]. To face these challenges, massive arrays and mm-wave frequencies emerge like potential candidates for including a large number of antennas in a small size with the possibility to focus the array beam in a precise direction in space [2]–[4]. In this context, an access point (AP) equipped with a massive array could be in principle used as a single-anchor node, i.e., a node whose position is *a-priori* known, permitting the mobile users to be aware of their positions, and, thus, enabling new applications such as those related to augmented reality and cyber-physical systems, as depicted in Fig. 1. Moreover, when operating at such high frequencies, the portable devices can also adopt massive arrays as the reduced wavelength permits to pack a large number of antennas in small spaces, as for example smartphones or tablets [5]–[7].

Different works deal with the derivation of the Cramer-Rao Lower Bound (CRLB) as a tool to investigate the ultimate performance of a localization system [8]–[14]. Notably, the CRLB can be considered as an asymptotic lower bound for all estimators and it can be asymptotically achieved, for example, by the maximum likelihood estimator (MLE) operating in high signal-to-noise ratio (SNR) regime. Therefore, here we aim at presenting the localization performance as a benchmark for real estimators without providing new localization techniques as done, for example, in some our previous works [15]. In [8], [9], the Position Error Bound (PEB) is derived for a wideband sensors network composed of several anchors and multipath effects are taken into account in the analysis. Nevertheless, in these works, beamforming strategies are completely neglected as anchors were considered equipped with a single antenna unable to perform beamsteering operations. Moreover, even if considered as a virtual array, anchors operate independently to each other as in multiple-input multiple-output (MIMO) systems. In our previous work [14], some preliminary results on positioning accuracy have been presented for different fractional bandwidth and spherical arrays.

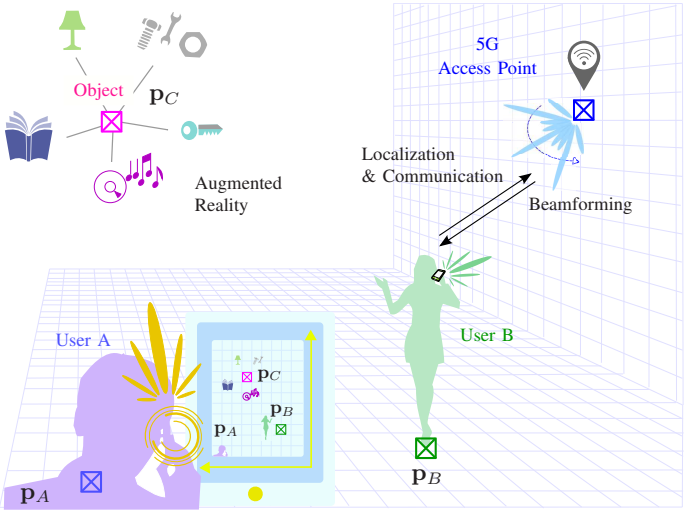

Fig. 1. Single AP localization scenario.

Stimulated by this framework, in this paper we propose a PEB study to compare the localization capabilities of mm-wave massive arrays operating different beamforming strategies. More specifically, *classical* and *random beamforming* will be compared in terms of positioning performance. In both cases, a phased array composed of phase shifters (PSs) is considered, as reported in Fig. 2. In the first strategy, all the beamforming weights are set in order to point towards a precise direction, e.g., the AP, while in the second one, the weights are randomly chosen. From a radiation pattern point-of-view, classical beamforming permits to accurately shape the radiation pattern radiation pattern with a main narrow beam in the intended direction. Differently, random beamforming results in a non-defined pattern shape but, at the same time, it permits to maintain a certain level of diversity gain while

Anna Guerra and Davide Dardari are with the Dipartimento di Ingegneria dell'Energia Elettrica e dell'Informazione "Guglielmo Marconi" - DEI, University of Bologna,Via Venezia 52, 47521 Cesena, ITALY.
(e-mail: anna.guerra3@unibo.it, davide.dardari@unibo.it).
Francesco Guidi is with CEA, LETI, MINATEC Campus, 38054 Grenoble, France. (e-mail: francesco.guidi@cea.fr).

keeping the architecture complexity lower. In fact, as shown in [16]–[18], where transmitarrays (i.e., a particular type of phased arrays consisting of a focal source illuminating a planar array) have been proposed, PSs are usually realized using switches. Therefore, as it is often unfeasible to obtain a continuous phase value ranging from 0° to 360° with real antennas, the resulting quantization errors should be taken into account in the analysis. Thus, this paper proposes a CRLB-based investigation on how a proper choice of the beamforming strategy can lead to different levels of localization accuracy and of array complexity.

The rest of the paper is organized as follows. In Sec. II we describe the considered array configurations, whereas in Sec. III we discussed an ad-hoc signal model for the analyzed multi-antennas schemes. Sec. IV shows the PEB derivation, where results are given in Sec. V. Final conclusions are successively drawn in Sec. VI.

II. Antenna Array Geometric Configuration

We consider a 3D localization scenario consisting of a N_{rx}-sized receiving array located in known position (i.e., $\mathbf{p}^{\text{r}} = [x_0^{\text{r}}, y_0^{\text{r}}, z_0^{\text{r}}]^{\text{T}} = [0,0,0]^{\text{T}}$) and a transmitting array with N_{tx} antennas whose position, $\mathbf{p}^{\text{t}} = [x_0^{\text{t}}, y_0^{\text{t}}, z_0^{\text{t}}]^{\text{T}} = [x,y,z]^{\text{T}}$, is to be inferred by the estimation process. We indicate with $\boldsymbol{\theta} = [\theta, \phi]^{\text{T}}$ the direction-of-arrival (DOA), i.e., the angle formed between the two arrays geometric centers. Moreover, if classical beamforming is considered, the steering angles will be indicated with $\boldsymbol{\theta}_0 = [\theta_0, \phi_0]^{\text{T}}$.

In both arrays, the antennas coordinates with respect to the array centroid can be expressed as

$$\mathbf{p}_{i/m}^{\text{t/r}}(\boldsymbol{\vartheta}^{\text{t/r}}) = \left[x_{i/m}^{\text{t/r}},\, y_{i/m}^{\text{t/r}},\, z_{i/m}^{\text{t/r}}\right]^{\text{T}} = \rho_{i/m}^{\text{t/r}}\, \mathbf{R}\left(\boldsymbol{\vartheta}^{\text{t/r}}\right)\, \mathbf{d}^{\text{T}}\left(\boldsymbol{\theta}_{i/m}^{\text{t/r}}\right) \tag{1}$$

with $i = 1,2,\ldots,N_{\text{tx}}$, $m = 1,2,\ldots,N_{\text{rx}}$ being the 1D transmitter (TX)/receiver (RX) antenna index, $\mathbf{R}\left(\boldsymbol{\vartheta}^{\text{t/r}}\right)$ being the 3D rotational matrix with $\boldsymbol{\vartheta}^{\text{t/r}} = \left[\vartheta^{\text{t/r}}, \varphi^{\text{t/r}}\right]^{\text{T}}$ being the transmitting/receiving array orientation with respect to its geometric center. The direction cosine in (1) is given by

$$\mathbf{d}\left(\boldsymbol{\theta}\right) = \left[\sin(\theta)\cos(\phi),\, \sin(\theta)\sin(\phi),\, \cos(\theta)\right]. \tag{2}$$

Finally, $\rho_{i/m}^{\text{t/r}} = \|\mathbf{p}_{i/m}^{\text{t/r}}(\boldsymbol{\vartheta}^{\text{t/r}}) - \mathbf{p}^{\text{t/r}}\|_2$ and $\boldsymbol{\theta}_{i/m}^{\text{t/r}} = \left[\theta_{i/m}^{\text{t/r}}, \phi_{i/m}^{\text{t/r}}\right]^{\text{T}}$ represent the transmitting/receiving spherical coordinates.

Having indicating with D the maximum diameter and with $d = \|\mathbf{p}^{\text{r}} - \mathbf{p}^{\text{t}}\|_2$ the distance between the two arrays, we suppose that they are sufficiently far from each other, i.e., $D \ll d$, in order to assume an identical angle of incidence at all the array antennas. Note that this hypothesis is especially verified at mm-wave where the array dimensions are very small thanks to the reduced wavelength. Given this assumption, it is possible to express the propagation delay and the amplitude between the mth receiving and the ith transmitting antenna, respectively, as

$$1)\ \tau_{im} \approx \tau + \tau_i^{\text{t}}(\boldsymbol{\theta}, \boldsymbol{\vartheta}^{\text{t}}) - \tau_m^{\text{r}}(\boldsymbol{\theta}, \boldsymbol{\vartheta}^{\text{r}}) \quad 2)\ a_{im} \approx a \tag{3}$$

where $\tau_{im} \triangleq \|\mathbf{p}_m^{\text{r}} - \mathbf{p}_i^{\text{t}}\|_2 / c$ is the time-of-arrival (TOA) between the mth receiving and the ith transmitting antenna,

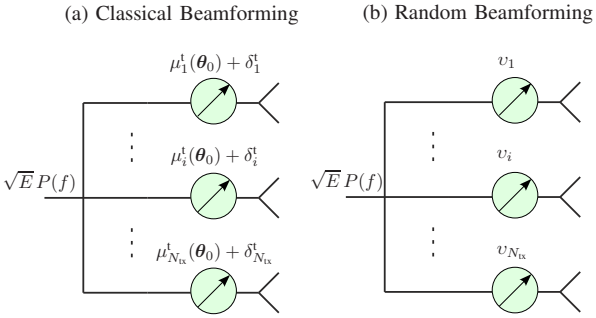

Fig. 2. Classical and random beamforming schemes.

$\tau \triangleq \|\mathbf{p}^{\text{r}} - \mathbf{p}^{\text{t}}\|_2 / c = d/c$ is the TOA between the arrays centers and $\tau_{i/m}^{\text{t/r}}(\boldsymbol{\theta}, \boldsymbol{\vartheta}^{\text{t/r}})$ is the transmitting/receiving inter-antenna delay given by

$$\tau_{i/m}^{\text{t/r}}(\boldsymbol{\theta}, \boldsymbol{\vartheta}^{\text{t/r}}) = \frac{1}{c}\, \mathbf{d}\left(\boldsymbol{\theta}\right)\, \mathbf{p}_{i/m}^{\text{t/r}}\left(\boldsymbol{\vartheta}^{\text{t/r}}\right) \tag{4}$$

with c being the speed of light.

III. Beamforming Schemes and Signal Model

In this section, the two array beamforming strategies present in Fig. 2 will be analysed from a signal processing point-of-view and by focusing on how the different signaling phasing schemes translate in different localization capabilities.

A. Transmitted Signal Model and Beamforming

The transmitted signal at the ith transmitting antenna is denoted with $g(t) = \sqrt{E}\,\Re\left\{p(t)\, e^{j\,2\,\pi\, f_{\text{c}} t}\right\}$ with $p(t)$ being the unitary energy equivalent low-pass signal, and f_{c} the carrier frequency. We consider a constraint on the total transmitted energy E_{tot} which is uniformly allocated among antennas, thus $E = E_{\text{tot}}/N_{\text{tx}}$ represents the normalized energy at each antenna element. We introduce the Fourier transform of $p(t)$ as $P(f) = \mathcal{F}\{p(t)\}$, with $\mathcal{F}\{\cdot\}$ denoting the Fourier transform operation in a suitable observation interval T_{obs}. For further convenience, the vector $\mathbf{p}(f) = P(f)\,\mathbf{1}_{N_{\text{tx}}\times 1}$ contains all the baseband transmitted signals with $\mathbf{1}_{N_{\text{tx}}\times 1}$ being a N_{tx}-sized vector of all ones.

In multi-antenna systems, beamforming is obtained by applying different weights at each array element. In classical beamforming, the objective of this operation is to coherently sum up signals towards the intended steering direction, i.e. $\boldsymbol{\theta}_0$. Considering the signal bandwidth W, when $W \ll f_{\text{c}}$ holds, this process can be realized using only PSs. The corresponding array structure is referred as phased array. Contrarily, in random beamforming, weights are randomly generated resulting in a non-directive radiation pattern but in an extremely low-complexity array design. In both cases, the beamforming weights are collected in a matrix that can be defined as

$$\mathbf{B} = \text{diag}\left(\omega_1,\, \omega_2,\, \ldots,\, \omega_i,\, \ldots\, \omega_{N_{\text{tx}}}\right) \tag{5}$$

where the ith PS generic element can be written as

$$\omega_i = \begin{cases} e^{j\,2\,\pi\, f_{\text{c}}\, \tau_i^{\text{t}}(\boldsymbol{\theta}_0)} = e^{j\mu_i^{\text{t}}(\boldsymbol{\theta}_0)} & \text{Classical Beam.} \\ e^{j\,\upsilon_i} & \text{Random Beam.} \end{cases} \tag{6}$$

with υ_i uniformly distributed between 0 and $2\,\pi$, i.e., $\upsilon_i \sim \mathcal{U}(0, 2\pi)$.

In addition, even when classical beamforming is adopted, some technological issues could induce errors in the beamforming vector resulting in an increased side-lobe level (SLL), decreased array maximum gain and angular resolution. In fact, in practical implementations, digitally controlled PSs are often adopted in place of their high-resolution analog counterparts inducing quantization errors, to be accounted for in the localization performance analysis [19].

In the presence of such non-perfect weights, a matrix accounting for non-idealities is introduced

$$\mathbf{Q} = \text{diag}\left(\varsigma_1,\, \varsigma_2,\, \ldots,\, \varsigma_i,\, \ldots,\, \varsigma_{N_{\text{tx}}}\right) \tag{7}$$

where ς_i takes into account the ith beamforming weight quantization error, i.e., $\varsigma_i = \exp\left(j\delta_i^{\text{t}}\right)$ with δ_i^{t} being the phase error. For further convenience, let indicate with $\tilde{\omega}_i = \exp\left(j(\mu_i^{\text{t}}(\boldsymbol{\theta}_0) + \delta_i^{\text{t}})\right)$ the quantized weights in classical beamforming; whereas $\tilde{\omega}_i = \omega_i$ in random beamforming.

B. Received Signal Model

All the received signals are gathered in a vector $\mathbf{r}(f) = [R_1(f),\, \ldots,\, R_m(f),\, \ldots,\, R_{N_{\text{rx}}}(f)]^{\text{T}}$, where $R_m(f) = \mathcal{F}\{r_m(t)\}$ is evaluated in T_{obs} and $r_m(t)$ is the equivalent low-pass received signal at the mth receiving antenna. Specifically, the received signal vector can be written as $\mathbf{r}(f) = \mathbf{x}(f) + \mathbf{n}(f)$, where the set of useful received signals is

$$\begin{aligned}\mathbf{x}(f) &= [X_1(f),\, \ldots,\, X_m(f),\, \ldots,\, X_{N_{\text{rx}}}(f)]^{\text{T}} \\ &= \sqrt{E}\; \mathbf{a}^{\text{r}}(f, \boldsymbol{\theta}, \boldsymbol{\vartheta}^{\text{r}})\; \mathbf{c}(f, \tau)\; \mathbf{A}^{\text{t}}(f, \boldsymbol{\theta}, \boldsymbol{\vartheta}^{\text{t}})\; \mathbf{Q}\; \mathbf{B}\; \mathbf{p}(f)\end{aligned} \tag{8}$$

and $\mathbf{n}(f) = [N_1(f),\, \ldots,\, N_m(f),\, \ldots,\, N_{N_{\text{rx}}}(f)]^{\text{T}}$ is the noise vector with $N_m(f) = \mathcal{F}\{n_m(t)\}$, with $n_m(t) \sim \mathcal{CN}(0, N_0)$ being a circularly symmetric, zero-mean, complex Gaussian noise. The receiving and transmitting direction matrices for the inter-antennas delays and TX orientation are

$$\mathbf{a}^{\text{r}}(f, \boldsymbol{\theta}, \boldsymbol{\vartheta}^{\text{r}}) = \left[e^{j\,\gamma_1^{\text{r}}},\, \ldots,\, e^{j\,\gamma_m^{\text{r}}},\, \ldots,\, e^{j\,\gamma_{N_{\text{rx}}}^{\text{r}}}\right]^{\text{T}} \tag{9}$$

$$\mathbf{A}^{\text{t}}(f, \boldsymbol{\theta}, \boldsymbol{\vartheta}^{\text{t}}) = \text{diag}\left(e^{-j\,\gamma_1^{\text{t}}},\, \ldots,\, e^{-j\,\gamma_i^{\text{t}}},\, \ldots,\, e^{-j\,\gamma_{N_{\text{tx}}}^{\text{t}}}\right) \tag{10}$$

with $\gamma_{i/m}^{\text{t/r}} = 2\pi\,(f + f_{\text{c}})\,\tau_{i/m}^{\text{t/r}}(\boldsymbol{\theta}, \boldsymbol{\vartheta}^{\text{t/r}})$. The channel vector is indicated with $\mathbf{c}(f, \tau) = \alpha\,\mathbf{1}_{1\times N_{\text{tx}}}$ being the $1 \times N_{\text{tx}}$, whose generic element is $\alpha = a\exp\left(-j\,2\,\pi\,(f + f_{\text{c}})\,\tau\right)$. For further convenience, define $\nu_t = E_{\text{t}}/N_0 = \nu\,N_{\text{tx}}$, with $\nu = E/N_0$. The SNR at each receiving antenna element is $\mathsf{SNR}_{\text{t}} = N_{\text{tx}}\mathsf{SNR}_1$, where $\mathsf{SNR}_1 = a^2\,\nu$ represents the SNR component related to the direct path between a generic couple of TX-RX antenna elements.

IV. Position Error Bound

In the following, we will derive the asymptotic limits of the TX position (i.e., $\mathbf{p}^{\text{t}}$) estimation error starting from the set of received waveforms $\mathbf{r}(f)$. Thus, we define the unknown parameters vector as $\boldsymbol{\psi} = \left[(\mathbf{p}^{\text{t}})^{\text{T}},\, a\right]^{\text{T}}$. We assume that an initial search between the TX and RX is conducted in order to coarsely infer the TX position and to allow the TX setting its own beamforming weights to point towards the RX in the case in which classical beamforming is operated.

The performance of any unbiased estimator $\widehat{\boldsymbol{\psi}} = \widehat{\boldsymbol{\psi}}\,(\mathbf{r}\,(f))$ can be bounded by the Cramér-Rao bound (CRB) defined as [20]

$$\mathbb{E}_{\mathbf{r},\boldsymbol{\psi}_{\text{r}}}\left\{\left[\widehat{\boldsymbol{\psi}} - \boldsymbol{\psi}\right]\left[\widehat{\boldsymbol{\psi}} - \boldsymbol{\psi}\right]^{\text{T}}\right\} \succeq \mathbf{J}_{\boldsymbol{\psi}}^{-1} = \mathsf{CRB}\,(\boldsymbol{\psi}) \tag{11}$$

where $\mathbf{J}_{\boldsymbol{\psi}}$ is the Fisher Information Matrix (FIM) given by

$$\mathbf{J}_{\boldsymbol{\psi}} \triangleq -\mathbb{E}_{\mathbf{r},\boldsymbol{\psi}_{\text{r}}}\left\{\nabla^2_{\boldsymbol{\psi}\boldsymbol{\psi}}\,\ln f\,(\mathbf{r}|\boldsymbol{\psi})\right\} = \begin{bmatrix} \mathbf{J}_{\mathbf{pp}} & \mathbf{J}_{\mathbf{p}a} \\ \mathbf{J}_{a\mathbf{p}} & J_{aa} \end{bmatrix} \tag{12}$$

with the symbol $\nabla^2_{\boldsymbol{\psi}\boldsymbol{\psi}} = \left(\partial^2/\partial\boldsymbol{\psi}\partial\boldsymbol{\psi}\right)$ indicating the second partial derivatives with respect to the elements in $\boldsymbol{\psi}$ and

$$\mathbf{J}_{\mathbf{pp}} = \begin{bmatrix} J_{xx} & J_{xy} & J_{xz} \\ J_{yx} & J_{yy} & J_{yz} \\ J_{zx} & J_{zy} & J_{zz} \end{bmatrix},\; \mathbf{J}_{\mathbf{p}a} = \begin{bmatrix} J_{xa} \\ J_{ya} \\ J_{za} \end{bmatrix}. \tag{13}$$

Since the observations at each receiving antenna element are independent, the log-likelihood function $\ln f\,(\mathbf{r}|\boldsymbol{\psi})$ can be written as

$$\ln f\,(\mathbf{r}|\boldsymbol{\psi}) \propto -\frac{1}{N_0}\sum_{m=1}^{N_{\text{rx}}}\int_W |R_m(f) - X_m(f)|^2\,df. \tag{14}$$

According to (12)-(14), it is possible to compute the elements of the FIMs as

$$\begin{aligned} J_{p_b\,p_a} &= 8\,\pi^2\,\nu\,a^2\sum_{mij}\Re\left\{\tilde{\omega}_{ij}\,\xi_{ij}\,\chi_{ij}(2)\right\}\nabla_{p_a}\left(\tau_{im}\right)\nabla_{p_b}\left(\tau_{jm}\right) \\ J_{a\,a} &= 2\,\nu\sum_{mij}\Re\left\{\tilde{\omega}_{ij}\,\xi_{ij}\,R_{ij}^{p}\left(\Delta\tau_{ij}\right)\right\} \\ J_{p_b\,a} &= 4\,\pi\,a\,\nu\sum_{mij}\Im\left\{\tilde{\omega}_{ij}\,\xi_{ij}\,\chi_{ij}(1)\right\}\nabla_{p_b}\left(\tau_{im}\right) = 0 \end{aligned} \tag{15}$$

where $p_{a/b}$ indicate two elements in the set $\{x,\, y,\, z\}$, $\sum_{mij} = \sum_{m=1}^{N_{\text{rx}}}\sum_{i=1}^{N_{\text{tx}}}\sum_{j=1}^{N_{\text{tx}}}$, $\tilde{\omega}_{ij} = \tilde{\omega}_i\,(\tilde{\omega}_j)^*$, $\xi_{ij} = e^{-j\,2\,\pi\,f_{\text{c}}\,\Delta\tau_{ij}}$ with $\Delta\tau_{ij} = \tau_{im} - \tau_{jm}$, and

$$\begin{aligned} \chi_{ij}(2) &= \int_W (f + f_{\text{c}})^2 e^{-j\,2\,\pi\,f\,\Delta\tau_{ij}}\,|P(f)|^2\,df \\ \chi_{ij}(1) &= \int_W (f + f_{\text{c}})\,e^{-j\,2\,\pi\,f\,\Delta\tau_{ij}}\,|P(f)|^2 df \\ R_{ij}^{p}(\Delta\tau_{ij}) &= \int_W e^{-j\,2\,\pi\,f\,\Delta\tau_{ij}}\,|P(f)|^2 df. \end{aligned} \tag{16}$$

The derivatives translating the TOA and DOA in position information can be expressed as

$$\nabla_p\left(\tau_{im}\right) = \frac{1}{c}\left\{c\,\nabla_p\left(\tau\right) + \nabla_p\left(\mathbf{d}\left(\boldsymbol{\theta}\right)\right)\left[\mathbf{p}_i^{\text{t}}(\boldsymbol{\vartheta}^{\text{t}}) - \mathbf{p}_m^{\text{t}}(\boldsymbol{\vartheta}^{\text{r}})\right]\right\} \tag{17}$$

with

$$\begin{aligned} \nabla_p\left(\mathbf{d}\left(\boldsymbol{\theta}\right)\right) = &\nabla_p\left(\theta\right)\cos(\theta)\begin{bmatrix} \cos(\phi) \\ \sin(\phi) \\ -\tan(\theta) \end{bmatrix}^{\text{T}} \\ &+ \nabla_p\left(\phi\right)\sin(\theta)\begin{bmatrix} -\sin(\phi) \\ \cos(\phi) \\ 0 \end{bmatrix}^{\text{T}}. \end{aligned} \tag{18}$$

$$\nabla_{\mathbf{pp}}(\tau_{im},\tau_{jm}) = \begin{bmatrix} \nabla_x(\tau_{im})\nabla_x(\tau_{jm}) & \nabla_x(\tau_{im})\nabla_y(\tau_{jm}) & \nabla_x(\tau_{im})\nabla_z(\tau_{jm}) \\ \dots & \nabla_y(\tau_{im})\nabla_y(\tau_{jm}) & \nabla_y(\tau_{im})\nabla_z(\tau_{jm}) \\ \dots & \dots & \nabla_z(\tau_{im})\nabla_z(\tau_{jm}) \end{bmatrix}$$
$$= \frac{d_{\text{ant}}^2}{(c\,y)^2} \begin{bmatrix} (m_x - i_x)(m_x - j_x) & \frac{y}{d_{\text{ant}}}(m_x - i_x) & (m_x - i_x)(j_z - m_z) \\ \dots & \frac{y^2}{d_{\text{ant}}^2} & \frac{y}{d_{\text{ant}}}(j_z - m_z) \\ \dots & \dots & (i_z - m_z)(j_z - m_z) \end{bmatrix} \tag{19}$$

Moreover, by further analyzing (15), one can notice the dependence of the FIM from the beamforming weights given by the coefficients $\tilde{\omega}_{ij}$.

Finally, by using the Schur complement, the PEB expression can be easily derived as

$$\mathsf{PEB} = \sqrt{\text{tr}\left(\mathsf{CRB}\left(\mathbf{p}^{\text{t}}\right)\right)} = \sqrt{\text{tr}\left(\left(\mathbf{J}_{\mathbf{pp}} - \mathbf{J}_{\mathbf{p}a}\; J_{aa}^{-1}\; \mathbf{J}_{\mathbf{p}a}^{\text{H}}\right)^{-1}\right)}$$
$$= \sqrt{\text{tr}\left(\mathbf{J}_{\mathbf{pp}}^{-1}\right)} \tag{20}$$

where $\text{tr}(\cdot)$ is the trace operation.

Equation (20) is a general bound valid for any beamforming strategy and accounting for signal weights quantization effects. Specialized expressions can be derived from (20) for specific cases to get insights on the key parameters affecting the performance as it will be done in the following.

A. Absence of Quantized Weights in Classical Beamforming

Here we provide an example on how the general expression (20) can be simplified in absence of beamforming weights errors. Given the FIM in (15), it can be easily found that for classical beamforming it is

$$\mathsf{PEB} = \sqrt{\text{tr}\left(\mathbf{G}^{-1}\,\breve{\mathbf{J}}_{\mathbf{pp}}^{-1}\right)} \tag{21}$$

where we have separated the effect of signal design $\breve{\mathbf{J}}_{\mathbf{pp}}$ (i.e., that related to (16)) from that of the geometry $\mathbf{G}$ (i.e., that related to (17)). Specifically for phased arrays, we have

$$\breve{\mathbf{J}}_{\mathbf{pp}} = 8\pi^2\,\mathsf{SNR}_1\left(\beta^2 + f_{\text{c}}^2\right) \tag{22}$$
$$\mathbf{G} = \sum_{mij} \nabla_{\mathbf{pp}}\left(\tau_{im},\tau_{jm}\right) \tag{23}$$

where $\nabla_{\mathbf{pp}}\left(\tau_{im},\tau_{jm}\right)$ is a 3×3 matrix and β^2 is the squared baseband effective bandwidth of $p(t)$.

The matrix $\mathbf{G}$ provides, through derivatives, the relationship between the TOA-DOA at each TX-RX antenna element couple and the TX position. To improve the comprehension of (21), in the next paragraph the particular case of planar arrays will be discussed considering a fixed orientation $\boldsymbol{\vartheta}^{\text{t}} = \boldsymbol{\vartheta}^{\text{r}} = [0,0]^{\text{T}}$.

1) Special Case: Planar Array: For squared arrays with antennas spaced of d_{ant}, we can compute a simplified version of (17). Specifically, it is possible to obtain:

$$\nabla_p\left(\tau_{im}\right) = \frac{1}{c}\left[c\,\nabla_p\left(\tau\right) + d_{\text{ant}}\left((i_x - m_x)\nabla_p(\phi)\right.\right.$$
$$\left.\left.+(m_z - i_z)\nabla_p(\theta)\right)\right] \tag{24}$$

with $m_x = m_z = -\frac{\sqrt{N_{\text{rx}}}}{2},\dots,\frac{\sqrt{N_{\text{rx}}}}{2}$ and $i_x = i_z = j_x = j_z = -\frac{\sqrt{N_{\text{tx}}}}{2},\dots,\frac{\sqrt{N_{\text{tx}}}}{2}$. From (24), it is straightforward to derive (19). Then, by considering the summations present in (22), it is possible to obtain the elements of the position CRB matrix as

$$\mathsf{CRB}\left(x\right) = \mathsf{CRB}\left(z\right) = \mathsf{CRB}_0\,\frac{12}{S}\frac{1}{N_{\text{tx}}\left(N_{\text{rx}}-1\right)}$$
$$\mathsf{CRB}\left(y\right) = \frac{\mathsf{CRB}_0}{N_{\text{tx}}\,N_{\text{rx}}} \tag{25}$$

where CRB_0 represents the CRB of the ranging error one would obtain using single antenna which can be written as

$$\mathsf{CRB}_0 = \frac{c^2}{8\pi^2\,\mathsf{SNR}_{\text{t}}\left(\beta^2 + f_{\text{c}}^2\right)} \tag{26}$$

and $S = A^{\text{r}}/y^2$ with $A^{\text{r}} = N_{\text{rx}}\,d_{\text{ant}}$.

From (25) it is possible to remark that the CRB of the estimation error in the y-coordinate is inversely proportional to N_{tx} and N_{rx}: in fact, the N_{tx} term accounts for the SNR enhancement due to the beamforming process while the N_{rx} term accounts for the number of independent measurements available at the RX.

V. Numerical Results

In this section, numerical results are reported considering the two discussed beamforming schemes. For what the antennas spatial deployment is regarded, planar arrays are accounted for as they represent the most conventional structure to be integrated in small-sized devices. Differently from Sec. IV-A1, here we compare results with fixed and averaged RX orientations, thus giving the possibility to appreciate the impact of the array rotation on the localization performance.

We consider a scenario with a single RX with the centroid placed in $\mathbf{p}^{\text{r}} = [0,0,0]^{\text{T}}$, and a TX located in $\mathbf{p}^{\text{t}} = [0,5,0]^{\text{T}}$ ($d = 5\,\text{m}$). As previously assumed, the RX has a perfect knowledge of the TX steering direction.

Results are obtained for $f_{\text{c}}{=}60\,\text{GHz}$ and $W{=}1\,\text{GHz}$ (the signal duration is $\tau_{\text{p}} = (1+\beta)/W = 1.6\,\text{ns}$) in free-space conditions. Root raised cosine (RRC) transmitted pulses centered at frequency $f_{\text{c}} = 60\,\text{GHz}$ and roll-off factor $\beta = 0.6$ are adopted, being compliant with the Federal Communications Commission (FCC) mask at 60 GHz [21]. A noise figure of $N_{\text{F}} = 4\,\text{dB}$ and a fixed transmitted power of $P_{\text{t}} = 10\,\text{mW}$ are considered, if not otherwise indicated.

The performance is evaluated in terms of PEB averaged over $N_{\text{cycle}} = 500$ Monte Carlo iterations. For each cycle, a different 3D RX array orientation is generated. The antennas are spaced apart of $d_{\text{ant}} = \lambda_L/2$, where $\lambda_L = c/f_L$ and

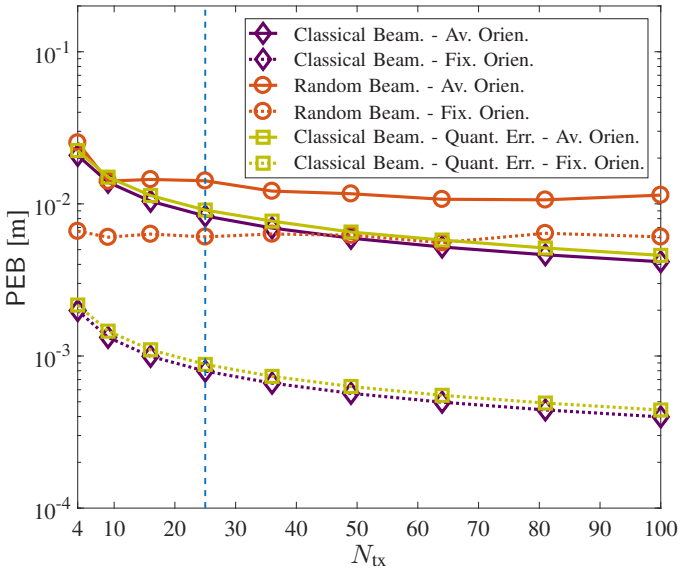

Fig. 3. Classical and random beamforming PEB *vs.* N_{tx}, $N_{\text{rx}} = 25$.

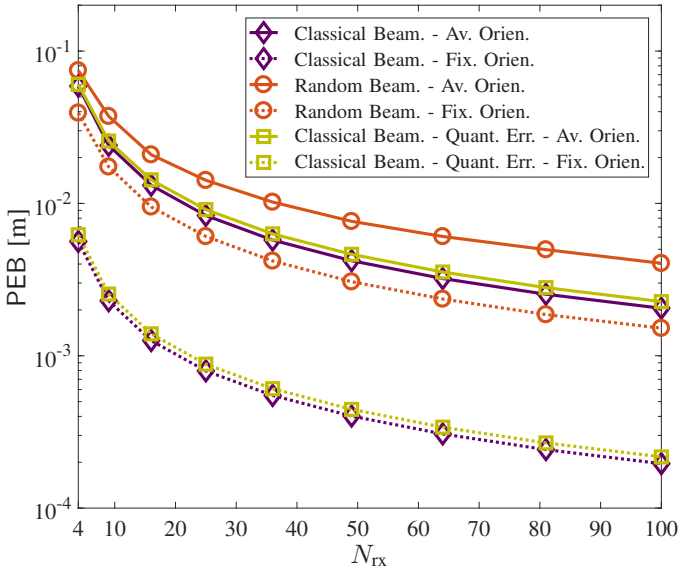

Fig. 4. Classical and random beamforming PEB *vs.* N_{rx}, $N_{\text{tx}} = 25$.

$f_L = f_c - W/2$. When present, the PSs quantization errors are $\delta_i^{\text{t}} \sim \mathcal{U}(-\pi/4, \pi/4)$ and the random beamforming weights $\upsilon_i \sim \mathcal{U}(0, 2\pi)$.

A. Results

Results have been obtained in free space conditions as a function of the number of antennas; of the beamforming schemes (i.e., classical *vs.* random); of the presence or absence of quantization errors; and as a function of arrays orientation.

In Fig. 3, the PEB performance is reported as a function of N_{tx}, for $N_{\text{rx}} = 25$ and averaged over different RX's orientations, apart for results refering to the fixed orientation (i.e., $\boldsymbol{\vartheta}^{\text{r}} = [0, 0]^{\text{T}}$). It can be observed that classical beamforming is very sensitive to the particular geometric configuration chosen when compared with its random counterpart, and performance can drastically decrease when a rotational angle is considered. On the other side, the impact of quantization errors is not much appreciable both in fixed and averaged RX orientations.

For what random beamforming is regarded, it shares the structure simplicity of phased arrays but it does not allow the formation of a high gain main beam pointing towards the RX, and thus, the positioning accuracy results degraded with respect to that achievable with classical beamforming. Nevertheless, as previously mentioned, it results more insensitive with respect to the RX orientation. Consequently, if the localization accuracy required by the application of interest is not so stringent, random beamforming can be an interesting option to guarantee both a sub-centimeter positioning accuracy (e.g., for $N_{\text{rx}} = 50$ and $N_{\text{tx}} = 25$, PEB ≈ 1 cm) and an easy implementation in future devices operating at mm-wave frequencies. For example, it could be employed for an initial coarse users localization estimation useful as a preliminary step before a precise beamforming operation. For what the number of TX antennas is concerned, it can be observed that the localization performance for $N_{\text{tx}} > 25$ is almost constant for all the configurations, and thus, it can be relaxed in order to guarantee an easy integration in portable devices.

In Fig. 4, the PEB results are reported as a function of the receiving antennas with N_{tx} fixed to 25. The same considerations drawn for Fig. 3 hold with the exception of those regarding the dependence on N_{rx}. Indeed, in this case, a higher number of antennas translates in a higher number of collected measurements and thus, in an increased localization accuracy.

VI. Conclusion

In this paper, we have considered a new scenario where a single-anchor localization exploiting mm-wave massive arrays has been put forth for next 5G applications. The theoretical PEB has been evaluated for different beamforming strategies, i.e., classical *vs.* random beamforming. Moreover, phase quantization errors and arrays orientation have been taken into account in the analysis.

From numerical results, we can conclude that classical beamforming permits to achieve a better localization performance thanks to the capability of focusing the power towards a precise direction in space; nevertheless, random beamforming attains a sub-centimeter accuracy even when the number of antennas is not extremely massive. Finally, the impact of quantization errors can be considered negligible. Consequently, whenever the localization requirements are not too stringent, it is possible to relax the implementation constraints (i.e., adoption of switches instead of analog PSs) without severely degrading the localization performance.

Acknowledgment

This work has been supported by the H2020 project XCycle (Grant 635975) and in part by the H2020-EU.1.3.2 IF-EF Marie-Curie project MAPS (Grant 659067).

REFERENCES

[1] R. Di Taranto *et al.*, "Location-aware communications for 5G networks: How location information can improve scalability, latency, and robustness of 5G," *IEEE Signal Process. Mag.*, vol. 31, no. 6, pp. 102–112, 2014.

[2] W. H. Chin, Z. Fan, and R. Haines, "Emerging technologies and research challenges for 5G wireless networks," *IEEE Wireless Commun.*, vol. 21, no. 2, pp. 106–112, 2014.

[3] E. G. Larsson *et al.*, "Massive mimo for next generation wireless systems," *IEEE Commun. Mag.*, vol. 52, no. 2, pp. 186–195, 2014.

[4] A. L. Swindlehurst *et al.*, "Millimeter-wave massive MIMO: The next wireless revolution?" *IEEE Commun. Mag.*, vol. 52, no. 9, pp. 56–62, 2014.

[5] S. M. Razavizadeh, M. Ahn, and I. Lee, "Three-dimensional beamforming: A new enabling technology for 5G wireless networks," *IEEE Signal Process. Mag.*, vol. 31, no. 6, pp. 94–101, 2014.

[6] K. Witrisal *et al.*, "High-accuracy localization for assisted living: 5G systems will turn multipath channels from foe to friend," *IEEE Signal Process. Mag.*, vol. 33, no. 2, pp. 59–70, 2016.

[7] N. Garcia *et al.*, "Direct localization for massive MIMO," *arXiv preprint arXiv:1607.00946*, 2016.

[8] Y. Shen and M. Z. Win, "On the accuracy of localization systems using wideband antenna arrays," *IEEE Trans. Commun.*, vol. 58, no. 1, pp. 270–280, 2010.

[9] ——, "Fundamental limits of wideband localizationpart I: A general framework," *IEEE Trans. Inf. Theory*, vol. 56, no. 10, pp. 4956–4980, 2010.

[10] Y. Han *et al.*, "Performance limits and geometric properties of array localization," *IEEE Trans. Inf. Theory*, vol. 62, no. 2, pp. 1054–1075, 2016.

[11] A. Shahmansoori *et al.*, "5G position and orientation estimation through millimeter wave MIMO," in *Proc. IEEE Global Conf. on Commun. (GLOBECOM) Workshops*, 2015, pp. 1–6.

[12] A. Mallat and L. Vandendorpe, "CRBs for the joint estimation of TOA and AOA in wideband MISO and MIMO systems: comparison with SISO and SIMO systems," in *Proc. IEEE Int. Conf. on Commun.*, 2009, pp. 1–6.

[13] A. Wang, L. Liu, and J. Zhang, "Low complexity direction of arrival (DoA) estimation for 2D massive MIMO systems," in *Proc. IEEE Global Conf. on Commun. (GLOBECOM) Workshops*, 2012, pp. 703–707.

[14] A. Guerra, F. Guidi, and D. Dardari, "Position and orientation error bound for wideband massive antenna arrays," in *Proc. IEEE Int. Conf. on Commun. Workshop (ICCW)*, 2015, pp. 853–858.

[15] F. Guidi *et al.*, "Joint energy detection and massive arrays design for localization and mapping," *IEEE Trans.Wireless Commun.*, To appear.

[16] H. Kaouach *et al.*, "Wideband low-loss linear and circular polarization transmit-arrays in V-band," *IEEE Trans. Antennas Propag.*, vol. 59, no. 7, pp. 2513–2523, 2011.

[17] A. Clemente *et al.*, "1-bit reconfigurable unit cell based on pin diodes for transmit-array applications in-band," *IEEE Trans. Antennas Propag.*, vol. 60, no. 5, pp. 2260–2269, 2012.

[18] ——, "Wideband 400-element electronically reconfigurable transmitarray in X band," *IEEE Trans. Antennas Propag.*, vol. 61, no. 10, pp. 5017–5027, 2013.

[19] F. Guidi, A. Guerra, and D. Dardari, "Personal mobile radars with millimeter-wave massive arrays for indoor mapping," *IEEE Trans. Mobile Comput.*, vol. 15, no. 6, pp. 1471–1484, 2016.

[20] H. L. Van Trees, *Detection, estimation, and modulation theory*. John Wiley & Sons, 2004.

[21] FCC, "Revision of Part 15 of the Commissions Rules Regarding Operation in the 57-64 GHz Band. August 2013."